Feedback-induced chaos and intensity-noise enhancement in vertical-cavity surface-emitting lasers

Joanne Y. Law and Govind P. Agrawal

The Institute of Optics and Rochester Theory Center, University of Rochester, Rochester, New York 14627

Received May 19, 1997; revised manuscript received August 29, 1997

We investigate numerically the effects of optical feedback on the intensity noise of vertical-cavity surface-emitting lasers (VCSEL's) under single-mode and two-mode operations. Our model includes transverse effects such as carrier diffusion and spatial hole-burning. Results indicate that the relative-intensity noise is relatively unaffected at low feedback levels except for a narrowing and enhancement of the relaxation-oscillation peak. At higher feedback levels, the VCSEL ceases to operate continuously, and its output becomes chaotic, following a period-doubling or a quasi-periodic route depending on the feedback level and the length of the external cavity. In the chaotic regime, the relative-intensity noise is enhanced by more than 20 dB. The critical feedback level at which the VCSEL output becomes chaotic depends on whether the laser operates in one or two transverse modes and how strongly these transverse modes are coupled through spatial hole-burning. © 1998 Optical Society of America [S0740-3224(98)00302-6]

OCIS codes: 140.1540, 140.3430, 140.2020, 140.5960.

1. INTRODUCTION

The most significant attributes of vertical-cavity surface-emitting lasers (VCSEL's) include a low threshold current, single-longitudinal-mode operation, a circular beam profile, high-speed-modulation capabilities, and wafer-scale integrability.[1,2] Because of these advantages, VCSEL's are attractive as compact light sources for applications in optical communications and interconnects. An important consideration for such applications is the behavior of VCSEL's under feedback conditions, since some light is invariably reflected back into the VCSEL. Indeed, linewidth narrowing and broadening,[3] threshold change,[4–6] mode hopping, and coherence collapse[7] have been experimentally observed. In particular, VCSEL's experience relative-intensity-noise (RIN) degradation under feedback conditions.[7] There are a number of studies on VCSEL performance under feedback conditions by means of models that neglect spatial effects.[8,9] Since VCSEL's have relatively large transverse dimensions, spatial effects such as spatial hole-burning and carrier diffusion are expected to be important, especially because VCSEL's often operate in several transverse modes at high injection currents.[2] Such spatial effects are also expected to play a role in determining VCSEL dynamic and noise characteristics under feedback conditions, particularly for the case of multimode operation where intermodal coupling induced by spatial hole-burning can affect device performance significantly. Indeed, we will see that details of the feedback dynamics as well as the feedback sensitivity depend considerably on the number and types of transverse modes in which a VCSEL operates simultaneously.

In this paper, we investigate numerically the RIN characteristics of VCSEL's under feedback conditions by means of a model that includes the spatial dependences of both the optical field and the carrier density. Both single-mode and two-mode operations are studied. Section 2 describes our model. Section 3 focuses on the study of feedback-induced RIN enhancement under single-mode operation. Section 4 studies two-mode operation with a disc-contact and ring-contact geometry, respectively. The RIN spectrum and temporal behavior at various feedback levels are investigated.

2. COMPUTER MODEL AND PARAMETERS

Assuming that the VCSEL can operate in two transverse modes simultaneously, the rate equations in the cylindrical coordinates are written as[10]

$$\frac{dE_i}{dt} = \frac{1}{2}(1 - i\alpha)[G_i(t) - \gamma_i]E_i + F_i(t) + \sum_{m=1}^{M} \kappa_m E_i(t - m\tau)\exp(im\omega_i\tau), \tag{1}$$

$$\frac{\partial N}{\partial t} = D\nabla_T^2 N + \frac{J(r, \phi)}{qd} - \frac{N}{\tau_e} - BN^2 - \frac{1}{d}\sum_{i=1}^{2} G_{\text{local}}|E_i(t)|^2|\psi_i(r, \phi)|^2, \tag{2}$$

where $E_i(t)$ is the amplitude of the ith transverse mode with the spatial distribution $\psi_i(r, \phi)$, $N(r, \phi, t)$ is the carrier density, α is the linewidth enhancement factor, $G_i(t)$ and γ_i are the gain and cavity loss for the ith mode, and ω_i is the frequency of the ith mode under solitary operation. In Eq. (2), τ_e is the carrier lifetime due to nonradiative recombination, D is the diffusion coefficient, B is the spontaneous recombination coefficient, d is the thickness of the active layer, and $J(r, \phi)$ is the injection-

current density. In the small-signal regime, the local gain $G_{\text{local}} = a_0 v_g (N - N_T)/(1 + \epsilon_{NL}|E_i|^2)$ is assumed to be linearly proportional to the local carrier density $N(r, \phi, t)$, where N_T is the carrier density at transparency, a_0 is the gain cross section, v_g is the group velocity, and ϵ_{NL} is the nonlinear-gain parameter. Note that the field E_i is normalized such that $|E_i|^2$ corresponds to the photon number in the ith mode.

The modal gain $G_i(t)$ for each mode in Eq. (1) is obtained by calculating the spatial overlap between the local-gain profile and the spatial intensity distribution $|\psi_i(r, \phi)|^2$ of that mode. It is given by

$$G_i(t) = \frac{\int_0^d \int_0^{2\pi} \int_0^{R_a} G_{\text{local}}(r, \phi, t)|\psi_i(r, \phi)|^2 \sin^2(\beta z) r\,dr\,d\phi\,dz}{\int_0^L \int_0^{2\pi} \int_0^{R} |\psi_i(r, \phi)|^2 \sin^2(\beta z) r\,dr\,d\phi\,dz}, \quad (3)$$

where R_a is the radius of the active region, R is the radius of the device, and L is the length of the VCSEL cavity. The propagation constant β is the same for all transverse modes since they are associated with the same longitudinal mode. Our model assumes that the local gain G_{local} is the same for all modes irrespective of their operating frequency. This assumption is justified since mode spacing ($\sim$100 GHz) is a small fraction of the gain bandwidth. The model also assumes that the feedback does not change the number and spatial distributions of the transverse modes associated with the VCSEL in the absence of feedback.

The effect of spontaneous emission is included by the Langevin noise term $F_i(t)$ in Eq. (1). It describes a Markoffian Gaussian random process with zero mean and δ function correlation such that[11]

$$\langle F_i(t) \rangle = 0, \quad (4)$$

$$\langle F_i(t_1) F_j^*(t_2) \rangle = R_{\text{sp}} \delta_{ij} \delta(t_1 - t_2), \quad (5)$$

where $R_{\text{sp}} = n_{\text{sp}} \gamma$ is the average rate of spontaneous emissions into a laser mode, and n_{sp} is the spontaneous emission factor related to the degree of population inversion.[12] For semiconductor lasers, an appropriate value of n_{sp} is 1.8.

Optical feedback through multiple round trips is taken into account by the summation in the last term on the right side of Eq. (1).[13] κ_m is the feedback parameter after m external-cavity round trips, each of duration τ, and M is the total number of round trips included in the model. The parameter κ_m has a form similar to that for edge-emitting lasers[14] and is given by

$$\kappa_m = \frac{1}{\tau_L} \frac{1 - R_2}{R_2} (-1)^{m-1} (\sqrt{R_2 R_{\text{ext}} \eta_c})^m, \quad (6)$$

where R_2 and R_{ext} are the output-mirror and external-mirror reflectivities, τ_L is the solitary-laser round-trip time, and η_c is the coupling efficiency of the returned light to the intracavity optical field. In general, η_c can be different for different modes. In this study, the feedback light is assumed to form a one-to-one image of the VCSEL aperture so that $\eta_c = 1$. The feedback phase for the ith mode after m external-cavity round trips is given by $m\omega_i\tau$. In general, cross coupling among different transverse modes should be included. However, cross coupling can be neglected if the VCSEL operates in two orthogonally polarized transverse modes. We focus in this paper on this specific case. The analysis can, however, be easily extended to the multimode case in which several modes have the same polarization.

Because of high reflectivities of VCSEL mirrors ($R_2 > 99\%$), it is essential to include multiple round trips in the external cavity even for $R_{\text{ext}} \sim 1\%$, in contrast with the case of edge-emitting lasers. The number of external-cavity round trips M used in simulations is the smallest integer for which $\kappa_M/\kappa_1 < 0.1$. This approximation neglects feedback terms whose power is smaller than 1% of the dominant feedback term. For comparison with previous work on edge-emitting lasers,[14] it is useful to define a feedback parameter F_{ext} that corresponds to a single round trip in the external cavity as

$$F_{\text{ext}} = \frac{1 - R_2}{R_2} \sqrt{R_2 R_{\text{ext}}}. \quad (7)$$

We will use this parameter while discussing our numerical results.

The field and carrier equations [Eqs. (1) and (2)] are integrated numerically by a finite-difference method in both the temporal and spatial domains. The accuracy is maintained by choosing spatial and temporal resolutions fine enough so that the numerical results do not change with a further decrease in step sizes. We use a temporal resolution of 0.1 ps and a spatial resolution of 0.1 μm along the radial direction.

The carrier-density equation requires an implicit solution in the radial direction due to the coupling introduced by the diffusion term. To solve for $N(r)$ at any given point in time, the spatial domain is divided evenly into 100 steps. The radial mesh runs from δr to $R = 10\ \mu$m, where $\delta r = 0.1\ \mu$m is the spatial resolution. The point $r = 0$ is excluded because of the singularity associated with the Laplacian term. The boundary conditions $N(0) = N(\delta r)$ and $N(R) = 0$ are used. Since the diffusion term involves a second-order derivative of $N(r)$, each $N(r)$ is coupled only to its nearest neighbors $N(r + \delta r)$ and $N(r - \delta r)$. Therefore, provided that the gain is a linear function of $N(r)$, the carrier equation can be cast into a tridiagonal matrix form, which can be easily inverted to obtain a solution for $N(r)$. In spite of the matrix inversion involved, the computer code is reasonably fast. A typical run of a 26-ns trajectory takes less than 5 min on an Ultra-1 workstation. The RIN characteristics

are calculated numerically by averaging over seven trajectories, each of duration 26 ns, resulting in a resolution of 38 MHz over a 20-GHz frequency range. The RIN spectra are smoothed slightly to reduce the impact of a relatively small number of trajectories used for performing an ensemble average.

Table 1. Device Parameters Used in Simulations

Parameter	Value
Cavity length L_{eff}	2 μm
Active-region thickness (3 QW's)	3×8 nm
Radius of device	10 μm
Radius of index-guiding region	4 μm
Diffusion constant D	30 cm^2/s
Nonradiative recombination time τ_e	5 ns
Bimolecular recombination coefficient B	1×10^{-10} cm^3/s
Refractive indices n_1, n_2	3.4, 3.5
Wavelength λ	0.875 μm
Gain cross-section a_0	2.0×10^{-16} cm^2
Group velocity v_g	8.8×10^9 cm/s
Carrier density at transparency N_T	2.2×10^{18} cm^{-3}
Linewidth enhancement factor α	3.0
Mirror reflectivities R_1, R_2	0.995
Internal loss α_{int}	20 cm^{-1}
Longitudinal confinement factor Γ_l	0.012
Nonlinear-gain parameter ϵ_{NL}	1×10^{-17} cm^3
External-cavity length L_{ext}	1 cm

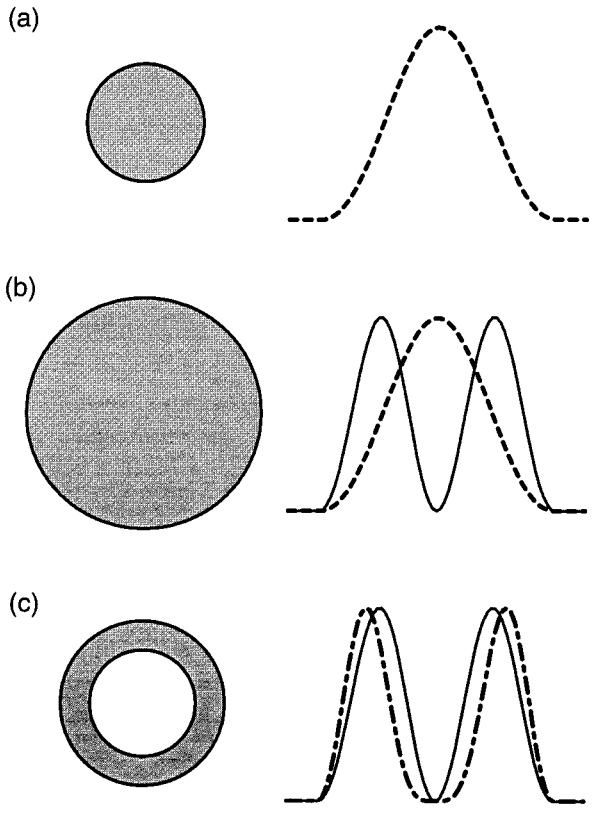

Fig. 1. Three types of electrical contact used and the radial intensity distributions of the transverse modes excited. (a) Narrow disc contact, (b) wide disc contact, and (c) ring contact. Dashed, solid and dotted-dashed curves represent the LP_{01}, LP_{11}, and LP_{21} transverse modes, respectively.

An index-guided VCSEL with cylindrical geometry (index guiding over 4-μm radius) is considered. The active region consists of three 8-nm quantum wells. Relevant device parameters are listed in Table 1. We first study how the shape of the electrical contact affects the transverse field distribution at a given current level in the absence of external influence. Our numerical results show that for the VCSEL whose parameters correspond to those given in Table 1, single-mode operation can be realized by use of a disc contact of 2-μm radius such that current is injected only over a small central part of the VCSEL top area. The LP_{01} mode is then preferentially excited. For two-mode operation, different transverse modes can be excited by two different contact geometries. Numerical simulations show that a 4-μm-radius disc contact excites the weakly overlapping LP_{01} and LP_{11} modes (weak-coupling case), and a ring contact of inner and outer radii of 1.8 and 2.8 μm excites the strongly overlapping LP_{11} and LP_{21} modes (strong-coupling case). These two cases are referred to as the disc-contact and ring-contact geometries in the following sections. A more detailed study of the effects of contact geometry on the lasing transverse-mode structures can be found in Refs. 10 and 15. The three types of electrical contacts used along with the radial intensity distributions of the transverse modes excited are shown in Fig. 1. The bias current is fixed at two times threshold throughout this study.

In our previous work, we have considered the effect of the external-cavity length on the feedback dynamics.[16] Similar to the results obtained for edge-emitting lasers,[14] it is found that feedback does not destabilize the cw operation for a very short external cavity ($L_{\text{ext}} < 100$ μm). In this paper, we focus on relatively long external cavities ($L_{\text{ext}} > 1$ mm) for which feedback leads to destabilization of the cw state. We choose $L_{\text{ext}} = 1$ cm and study the temporal behavior as well as the RIN spectrum at various feedback levels. The relative-power spectrum without the inclusion of spontaneous emission is also calculated to determine the origin of the RIN enhancement. We will refer to the relative-intensity spectrum with the inclusion of noise as the RIN spectrum and that without noise as the relative-power spectrum.

3. SINGLE-MODE OPERATION

This section considers a VCSEL forced to operate in a single transverse mode by use of a 2-μm-radius disc contact. A series of temporal traces showing the output power as a function of time in a 1.5-ns temporal window and the RIN spectra (bold curves) for six different values of the feedback parameter are shown in Fig. 2 and Fig. 3, respectively. The temporal traces are obtained with the Langevin noise term left out (no spontaneous emission) to show the feedback-induced nonlinear dynamics without fluctuations induced by the spontaneous emission noise. The corresponding relative-power spectra are also shown as light traces in Fig. 3 for comparison. In Fig. 3(a) and Fig. 3(e), the relative-power spectrum (without noise) contains only a dc component, and hence the light lines are not visible. Figure 3(a) shows the RIN spectrum in the

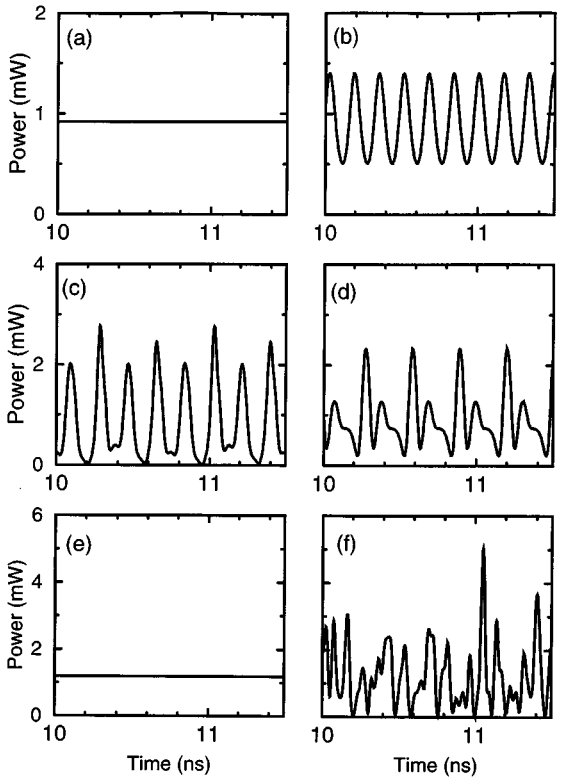

Fig. 2. Temporal evolution of the output power under single-mode operation for several feedback levels. (a) $F_{ext} = 0$, (b) $F_{ext} = 1.6 \times 10^{-4}$, (c) $F_{ext} = 5 \times 10^{-4}$, (d) $F_{ext} = 8.9 \times 10^{-4}$, (e) $F_{ext} = 1.6 \times 10^{-3}$, and (f) $F_{ext} = 2.8 \times 10^{-3}$.

absence of feedback ($F_{ext} = 0$). The peak near 6 GHz corresponds to the well-known relaxation-oscillation frequency.

Under weak feedback conditions ($F_{ext} < 1.3 \times 10^{-4}$), the laser retains the stable cw operation, and the RIN spectrum is relatively unchanged, although both the position and the amplitude of the relaxation-oscillation peak change. The increase in the relaxation-oscillation peak amplitude indicates that the optical feedback affects the damping of the relaxation oscillations. Eventually, as the feedback increases, the relaxation oscillations would become undamped at a certain feedback level, and the laser would cease to operate continuously. This scenario is indeed what is found to occur in our numerical simulation. For the VCSEL parameters used in our numerical simulations, the cw state becomes unstable for $F_{ext} > 1.3 \times 10^{-4}$. At $F_{ext} = 1.6 \times 10^{-4}$, the laser exhibits feedback-induced self-pulsations [see Fig. 2(b)] at the relaxation-oscillation frequency. The RIN spectrum therefore shows peaks at the self-pulsing frequency and its harmonics. With a further increase in F_{ext}, the VCSEL output becomes chaotic following a period-doubling route. As an example, Fig. 2(c) shows period-four oscillations. Interestingly enough, when spontaneous noise is included in the calculations, the RIN spectrum shown as bold curves in Fig. 3(c) corresponds to a period-doubling bifurcation. It is difficult to judge whether spontaneous-emission noise modifies the deterministic nonlinear dynamics or simply obscures it through spectral broadening, although the former case appears to be more likely in Fig. 3(c). Nonetheless, it is found that the feedback eventually forces the laser to enter a chaotic regime following a period-doubling route. The laser output becomes chaotic for $F_{ext} > 5.5 \times 10^{-4}$.

It is well known that a nonlinear chaotic system may have "windows" in the parameter space in which the chaotic behavior is replaced by periodic or even cw operation. The VCSEL under external feedback is found to be such a nonlinear system. The chaos abruptly ends for $F_{ext} > 8.8 \times 10^{-4}$, and the VCSEL makes a transition to a new cw state. Our results indicate that spontaneous emission affects both the location and the width of the chaotic window. Just after the laser exits the chaotic regime, period-two oscillations with a highly distorted wave form are observed at $F_{ext} = 8.9 \times 10^{-4}$ in the absence of spontaneous emission [see Fig. 2(d)]. Although the relative-power spectrum without noise shows a series of peaks at the dominant frequency (~4 GHz) and its harmonics, a broadly peaked RIN spectrum is observed with the inclusion of noise [Fig. 3(d)]. These results suggest that the inclusion of spontaneous noise changes the dynamics observed in Fig. 2(d) such that the power variations are no longer periodic with time, and the chaotic regime is extended to a larger range of feedback values. Since chaos is known to show sensitive dependence on the initial conditions, it is not surprising that stochastic

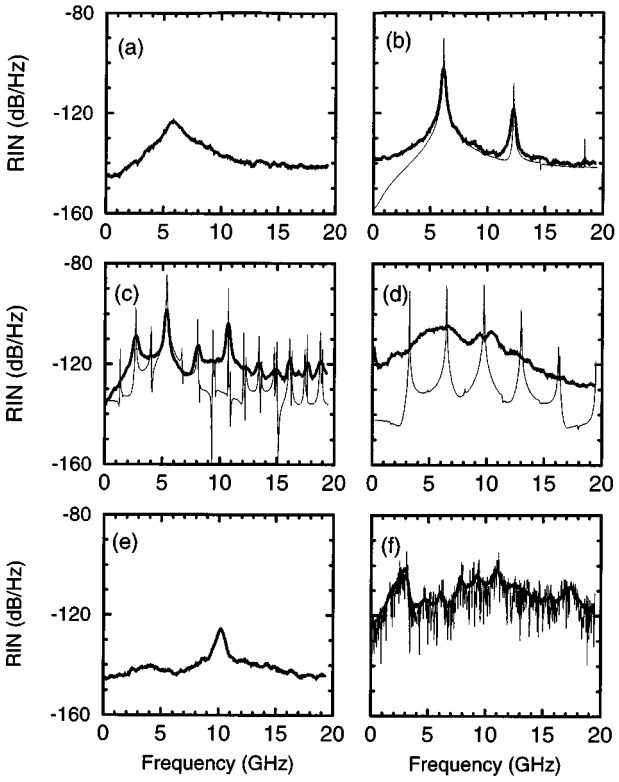

Fig. 3. RIN spectra (thick solid curves) under single-mode operation for several feedback parameters corresponding to those used in Fig. 2. The thin solid curves show the relative-power spectra corresponding to the temporal traces shown in Fig. 2 when spontaneous emission is neglected. The feedback levels used are (a) $F_{ext} = 0$, (b) $F_{ext} = 1.6 \times 10^{-4}$, (c) $F_{ext} = 5 \times 10^{-4}$, (d) $F_{ext} = 8.9 \times 10^{-4}$, (e) $F_{ext} = 1.6 \times 10^{-3}$, and (f) $F_{ext} = 2.8 \times 10^{-3}$.

noise can change the behavior of the laser considerably when operating close to the boundaries of the chaotic regime.

Under strong feedback conditions, it is found that stable cw operation of the VCSEL is possible for a small range of feedback values. Figure 2(e) shows the cw output occurring at $F_{ext} = 1.6 \times 10^{-3}$. The corresponding RIN spectrum shown in Fig. 3(e) exhibits a peak at 10 GHz. If this peak is interpreted as the relaxation-oscillation frequency, then it has increased by 4 GHz relative to the case of no feedback, and it is not obvious what leads to such a large change, since the power increases by only ~30% in Fig. 2(e), an increase too small to explain the large shift in the frequency. It is difficult to carry out a small-signal analysis because of a relatively high feedback level and the need for including multiple round trips in the external cavity. The absence of any temporal power oscillations for the case of Fig. 3(e) seems to exclude the interpretation of the 10-GHz peak as a beat frequency.

The cw state becomes unstable again when F_{ext} exceeds 2.3×10^{-3} and the laser output becomes chaotic as seen in Fig. 3(f). However, the laser enters the chaotic regime via a quasi-periodic route in contrast with the period-doubling route observed during the first onset of chaos. The mixing and beating of the 4- and 10-GHz frequency components generated many new frequencies, as seen in Fig. 3(f). The quasi-periodic route to chaos has also been observed in edge-emitting semiconductor lasers.[17] The transition to chaos is responsible for the drastic increase (by >20 dB) in the RIN seen in Fig. 3(f). Comparing Figs. 3(e) and 3(f), we can conclude that the RIN enhancement in this case is solely due to deterministic chaos. We should stress that a complete characterization of chaos would require further tests related to the Lyapunov exponent and the chaos dimension.

The RIN and relative-power spectra in Fig. 3 do not show any peaks at the external-cavity mode spacing $\Delta\nu_{ext} = c/2L_{ext}$. The most likely reason for their absence is that $\Delta\nu_{ext} = 15$ GHz for $L_{ext} = 1$ cm. This frequency is considerably larger than the relaxation-oscillation frequency of the VCSEL, which acts as an effective cut-off frequency above which the VCSEL response is weak. To study the interplay between the relaxation-oscillation frequency and $\Delta\nu_{ext}$, we have repeated our calculations for longer external cavities. It is found that the for $L_{ext} > 3$ cm, the VCSEL undergoes a quasi-periodic route to chaos, and the RIN spectra show strong peaks not only at the relaxation-oscillation frequency but also at $\Delta\nu_{ext}$ and its harmonics. Moreover, these peaks appear at lower and lower feedback levels as L_{ext} increases. For instance, these peaks set in for $F_{ext} > 1 \times 10^{-4}$ for $L_{ext} = 10$ cm. Since $\Delta\nu_{ext}$ is smaller than the relaxation-oscillation frequency for $L_{ext} > 3$ cm, the VCSEL can respond quite strongly at this frequency. The beating and mixing of the relaxation-oscillation frequency and the external-cavity modes induce chaos through a quasi-periodic route. The cw windows also become narrower, and disappear completely for external-cavity lengths of 10 cm or more.

We have investigated the effect of feedback phase ($\omega_i\tau$) on the laser dynamics by varying L_{ext} on a wavelength scale. It is found that although quantitative details of the feedback dynamics are sensitive to the feedback, similar qualitative features occur independent of the feedback phase, i.e., self-pulsations, route to chaos, and cw windows are consistently observed.

To understand the role of diffusion on the feedback-induced dynamics, we have varied the diffusion coefficient in the range $D = 0-30$ cm^2/s. In general, the feedback levels at which self-pulsations and chaos occur in Fig. 2 change with D. However, carrier diffusion does not alter the main qualitative feature that feedback leads to chaos following a period-doubling or a quasi-periodic route. Spectral features in Fig. 3 are also significantly affected by diffusion. Generally speaking, spectral peaks become narrower and much more pronounced as the diffusion coefficient decreases.

4. TWO-MODE OPERATION

A. Weak-Coupling Case

We first consider the weak-coupling case of two-mode operation realized with a 4-μm disc contact. Since the LP_{01} and LP_{11} modes overlap little spatially, they obtain most of the gain from the carrier density at different locations, resulting in weak coupling with nearly the same mode powers. The temporal evolution of the LP_{01} and LP_{11} mode powers are shown by the solid and dashed curves in Fig. 4, and the corresponding RIN spectra of the total

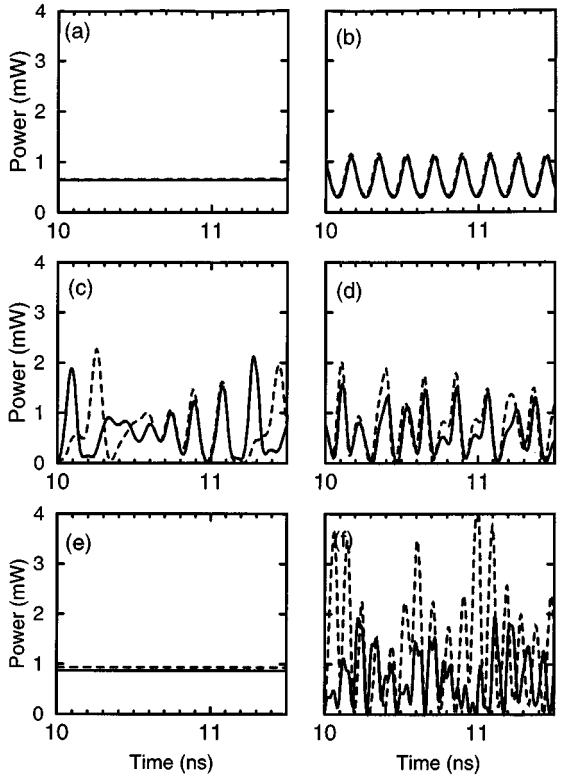

Fig. 4. Temporal evolution of the output power under two-mode operation with a 4-μm disc contact (weak coupling) for several feedback levels. Solid and dashed curves represent the LP_{01} and LP_{11} modes, respectively. (a) $F_{ext} = 0$, (b) $F_{ext} = 1.6 \times 10^{-4}$, (c) $F_{ext} = 5 \times 10^{-4}$, (d) $F_{ext} = 8.9 \times 10^{-4}$, (e) $F_{ext} = 1.6 \times 10^{-3}$, and (f) $F_{ext} = 2.8 \times 10^{-3}$.

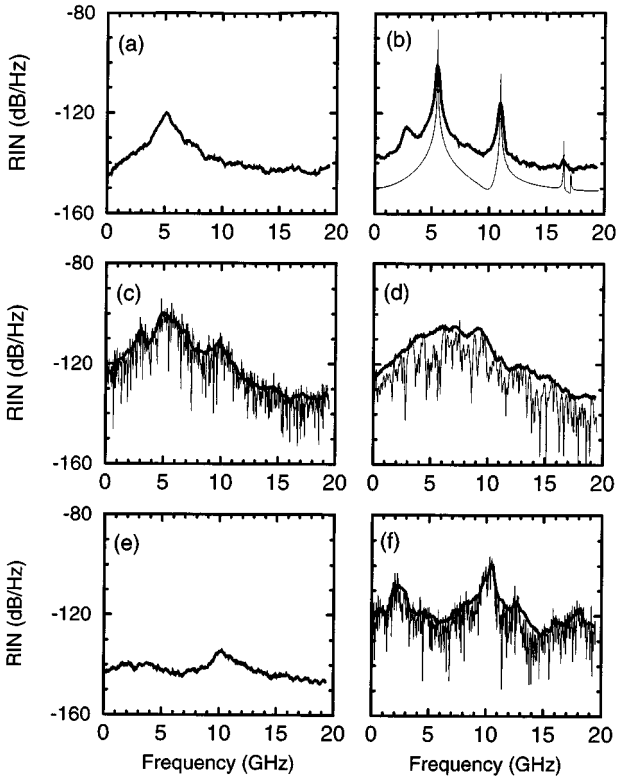

Fig. 5. RIN spectra (bold curves) for the total power under two-mode operation with a 4-μm disc contact (weak coupling). The thin solid curves show the relative-power spectra corresponding to the temporal traces shown in Fig. 4 when spontaneous emission is neglected. The feedback levels used are (a) $F_{ext} = 0$, (b) $F_{ext} = 1.6 \times 10^{-4}$, (c) $F_{ext} = 5 \times 10^{-4}$, (d) $F_{ext} = 8.9 \times 10^{-4}$, (e) $F_{ext} = 1.6 \times 10^{-3}$, and (f) $F_{ext} = 2.8 \times 10^{-3}$.

power are shown in Fig. 5. (Mode-partition noise issues are not considered in this paper. For a discussion of mode-partition noise under solitary conditions, see Ref. 18.) Under weak feedback conditions, the changes in the RIN spectrum with feedback are qualitatively similar to those of the single-mode case. More specifically, an increase in the relaxation-oscillation peak of ~10 dB is observed for $F_{ext} < 1 \times 10^{-4}$. As F_{ext} is increased, feedback results in undamped relaxation oscillations and chaos via a period-doubling route. As seen in Fig. 4(b), both modes oscillate in phase when the laser enters the self-pulsing regime. However, Fig. 4(c) shows that the chaotic pattern for the two modes are not synchronized. This is not surprising in view of the weak coupling between the two modes, since they can operate independently. A comparison of Fig. 2(c) and Fig. 4(c) shows that weak intermodal coupling leads to an early onset of deterministic chaos, resulting in significant RIN enhancement at a lower feedback level of only $F_{ext} \sim 5 \times 10^{-4}$ compared with the single-mode case. This early onset of chaos is contrary to the lower degree of sensitivity toward feedback for multimode edge-emitting lasers.[14] The difference can be understood in view of the strong coupling among the longitudinal modes in an edge-emitting laser, since these modes generally have identical spatial distributions. Our results suggest that the strength of intermodal coupling plays a major role in determining feedback-induced dynamics and the extent of the RIN enhancement. Our results for the strong-coupling case discussed below support this conclusion.

Under strong feedback conditions, the VCSEL can enter the cw regime [see Fig. 4(e)], and the RIN spectrum seen in Fig. 5(e) exhibits a peak at 10 GHz, similar to the single-mode case. Further increase in F_{ext} destabilizes the cw state once again and leads to chaos [Fig. 4(f)]. Similar to the single-mode case, the laser enters this second chaotic regime through a quasi-periodic route. The corresponding RIN spectrum shown in Fig. 5(f) exhibits a peak near 2 GHz together with other peaks resulting from the beating of 2-GHz and 10-GHz components.

B. Strong-Coupling Case

We next consider the strong-coupling case of the two-mode operation realized with a ring contact. We can excite the LP_{11} and the LP_{21} modes, whose spatial profiles overlap considerably. The temporal evolution for the LP_{11} and LP_{21} mode powers at various feedback levels are shown in Fig. 6, and the corresponding RIN spectra for the total power are shown in Fig. 7. Figures 6 and 7 should be compared with Figs. 4 and 5 (weak-coupling case) and Figs. 2 and 3 (single-mode case) to see the effect of intermodal coupling. It is found that the onset of self-pulsations and the associated RIN enhancement are delayed to higher feedback values (~5 times larger) compared with the case of single-mode operation as seen in

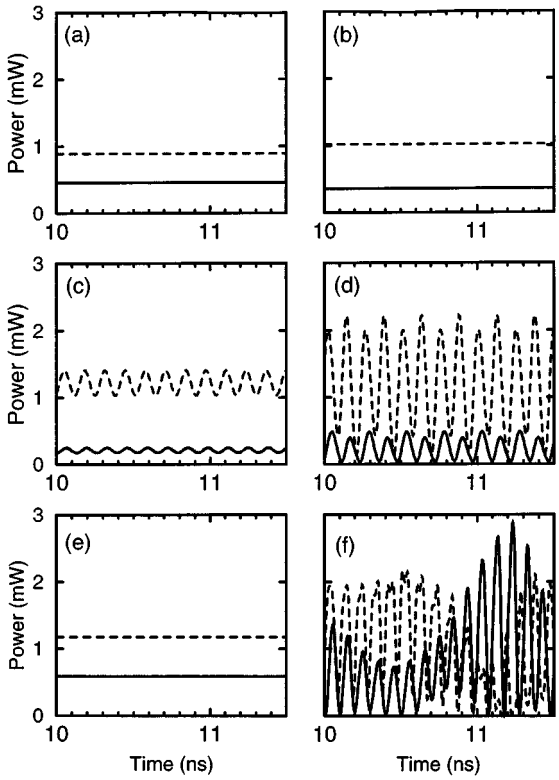

Fig. 6. Temporal evolution of the output power under two-mode operation with a ring contact (strong coupling) for several feedback levels. Solid and dashed curves represent the LP_{11} and LP_{21} modes, respectively. (a) $F_{ext} = 0$, (b) $F_{ext} = 1.6 \times 10^{-4}$, (c) $F_{ext} = 5 \times 10^{-4}$, (d) $F_{ext} = 8.9 \times 10^{-4}$, (e) $F_{ext} = 1.6 \times 10^{-3}$, and (f) $F_{ext} = 2.8 \times 10^{-3}$.

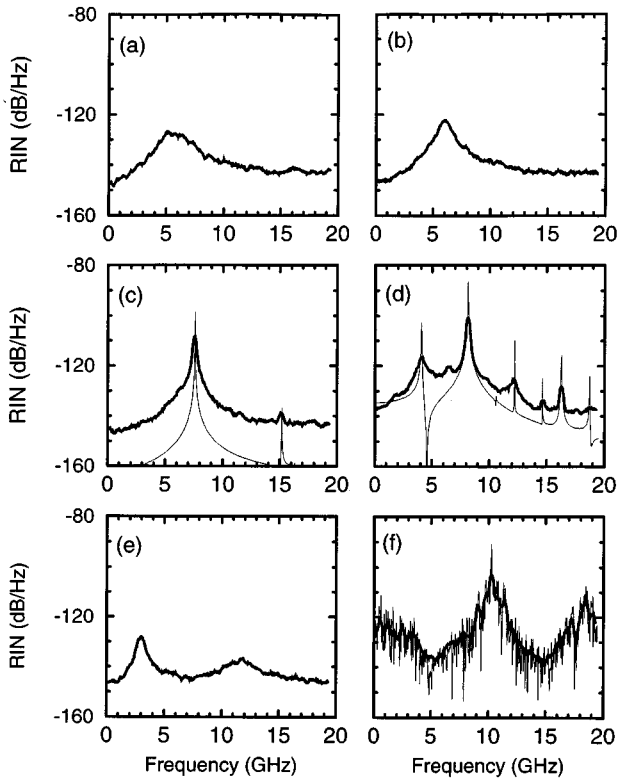

Fig. 7. RIN spectra (thick solid curves) for the total power under two-mode operation with a ring contact (strong coupling). The thin solid curves show the relative-power spectra corresponding to the temporal traces shown in Fig. 6 when spontaneous emission is neglected. (a) $F_{ext} = 0$, (b) $F_{ext} = 1.6 \times 10^{-4}$, (c) $F_{ext} = 5 \times 10^{-4}$, (d) $F_{ext} = 8.9 \times 10^{-4}$, (e) $F_{ext} = 1.6 \times 10^{-3}$, and (f) $F_{ext} = 2.8 \times 10^{-3}$.

Figs. 6(c) and 7(c). Further, the RIN enhancement due to the onset of deterministic chaos under strong feedback is reduced by ~10 dB. This reduction in sensitivity toward feedback is attributed to strong intermodal coupling effects. Since the two modes overlap strongly, spatial hole-burning results in strong intermodal coupling such that higher feedback levels are required to destabilize the cw operation of both modes simultaneously. Similar results were obtained in our previous study of optically injected VCSEL's, indicating that strong intermodal coupling can also reduce the sensitivity of VCSEL's toward external injection, in terms of both locking and nonlocking aspects.[19]

5. CONCLUSIONS

We have studied the change in the RIN characteristics of VCSEL's induced by external optical feedback, under both single-mode and two-mode operation. It is found that feedback can result in a significant RIN enhancement by as much as 20 dB or more depending on the feedback strength. Under weak feedback conditions, the increase in the relaxation-oscillation peak height is due to feedback-induced changes in the damping of the relaxation oscillations and has a stochastic origin. However, under strong feedback conditions, the RIN enhancement of more than 20 dB originates from deterministic chaos induced by feedback. The destabilization of the cw operation also leads to significant changes in the structure of the RIN spectrum. We also find that the chaos develops following a period-doubling or a quasi-periodic route depending on the feedback strength and the external-cavity length.

Similar qualitative changes of the RIN spectrum with feedback are observed for single-mode and two-mode operations. However, we find that strong intermodal coupling reduces the destabilizing effects of feedback and delays the onset of self-pulsations and chaos. Moreover, the RIN enhancement in the chaotic regime is reduced considerably. These results suggest that if feedback insensitivity is the most critical design issue, a ring contact is better than a disc contact.

ACKNOWLEDGMENTS

The authors thank Guido H. M. van Tartwijk for detailed discussions. This work is partially supported by the U.S. Army Research office and by the National Science Foundation under grant PHY94-15583.

REFERENCES

1. C. J. Chang-Hasnain, in *Semiconductor Lasers: Past, Present and Future*, G. P. Agrawal, ed. (American Institute of Physics, Woodbury, New York, 1995), Chap. 5.
2. C. J. Chang-Hasnain, J. P. Harbison, G. Hasnain, A. C. Von Lehmen, and N. G. Stoffel, "Dynamic, polarization and transverse mode characteristics of VCSELs," IEEE J. Quantum Electron. **27**, 1402–1408 (1991).
3. Y. C. Chong and Y. H. Lee, "Spectral characteristics of VCSEL with external optical feedback," IEEE Photon. Technol. Lett. **3**, 597–599 (1991).
4. U. Fiedler, "Design of VCSEL's for feedback insensitive data transmission and external cavity active mode-locking," IEEE J. Sel. Top. Quantum Electron. **1**, 442–449 (1995).
5. M. A. Hadley, G. C. Wilson, K. Y. Lau, and J. S. Smith, "High single-transverse-mode output from external-cavity surface-emitting laser diodes," Appl. Phys. Lett. **63**, 1607–1609 (1993).
6. G. C. Wilson, M. A. Hadley, J. S. Smith, and K. Y. Lau, "High single-mode output power from compact external microcavity surface-emitting laser diode," Appl. Phys. Lett. **63**, 3265–3267 (1993).
7. K. P. Ho, J. D. Walker, and J. M. Kahn, "External optical feedback effects on intensity noise of vertical-cavity surface-emitting lasers," IEEE J. Quantum Electron. **5**, 892–895 (1993).
8. H. M. Chen, K. Tai, K. F. Huang, Y. H. Kao, and J. D. Wynn, "Instability in SEL due to external optical feedback," J. Appl. Phys. **73**, 16–20 (1993).
9. J. P. Zhang, "Numerical simulation for VCSEL with external optical feedback," Microw. Opt. Technol. Lett. **7**, 359–361 (1994).
10. A. Valle, J. Sarma, and K. A. Shore, "Spatial hole-burning effects on the dynamics of vertical-cavity surface-emitting laser diodes," IEEE J. Quantum Electron. **31**, 1423–1431 (1995).
11. N. G. van Kampen, *Stochastic Processes in Physics and Chemistry* (North-Holland, Amsterdam, 1981).
12. G. P. Agrawal and N. K. Dutta, *Semiconductor Lasers*, 2nd ed. (Van Nostrand Reinhold, New York, 1993).
13. R. Lang and K. Kobayashi, "External optical feedback effects on semiconductor injection laser properties," IEEE J. Quantum Electron. **16**, 327–355 (1980).
14. A. T. Ryan, G. P. Agrawal, G. R. Gray, and E. C. Cage, "Optical-feedback-induced chaos and its control in multimode semiconductor lasers," IEEE J. Quantum Electron. **30**, 668–679 (1994).

15. C. H. Chong and J. Sarma, "Lasing mode selection in vertical-cavity surface-emitting laser diodes," IEEE Photon. Technol. Lett. **5**, 761–764 (1993).
16. J. Y. Law and G. P. Agrawal, "Effects of optical feedback on static and dynamic characteristics of vertical-cavity surface-emitting lasers," IEEE J. Sel. Top. Quantum Electron. **3**, 353–358 (1997).
17. J. Mørk, J. Mark, and B. Tromborg, "Route to chaos and competition between relaxation oscillations for a semiconductor laser with optical feedback," Phys. Rev. Lett. **65**, 1999–2002 (1990).
18. J. Y. Law and G. P. Agrawal, "Mode-partition noise in vertical-cavity surface-emitting laser," IEEE Photonics Technol. Lett. **9**, 437–439 (1997).
19. J. Y. Law, G. H. M. van Tartwijk, and G. P. Agrawal, "Effects of transverse-mode competition on injection dynamics in vertical-cavity surface-emitting lasers," Quantum Semiclass. Opt. **9**, 737–747 (1997).